ACS APPLIED MATERIALS & INTERFACES

Research Article

Cite This: ACS Appl. Mater. Interfaces 2019, 11, 24435−24446

www.acsami.org

Supramolecular Self-Assembly of 3D Conductive Cellulose Nanofiber Aerogels for Flexible Supercapacitors and Ultrasensitive Sensors

Duan-Chao Wang,[†] Hou-Yong Yu,[*,†,‡] Dongming Qi,[†] Mohankandhasamy Ramasamy,[‡] Juming Yao,[†] Feng Tang,[†] Kam (Michael) Chiu Tam,[*,‡] and Qingqing Ni[†,§]

[†]College of Materials and Textile, Zhejiang Sci-Tech University, Xiasha Higher Education Park Avenue 2 No. 928, Hangzhou 310018, China

[‡]Department of Chemical Engineering, Waterloo Institute for Nanotechnology, University of Waterloo, 200 University Avenue West, Waterloo, Ontario N2L 3G1, Canada

[§]Department of Mechanical Engineering and Robotics, Shinshu University, Tokida, Ueda 386-8576, Japan

Supporting Information

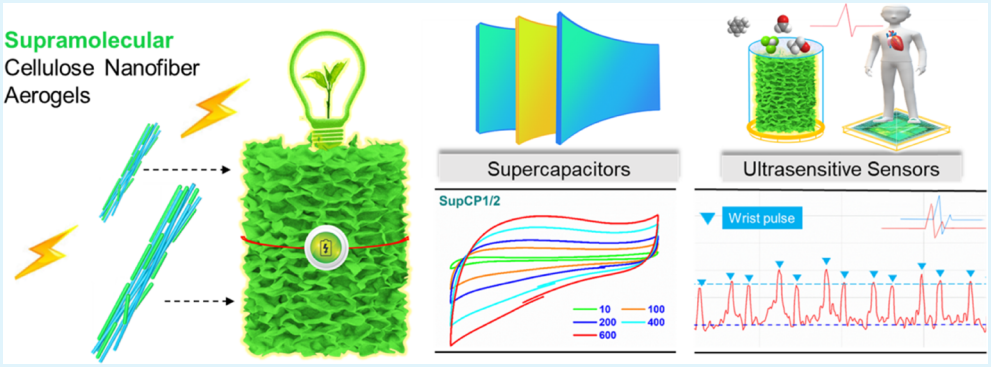

ABSTRACT: Nature employs supramolecular self-assembly to organize many molecularly complex structures. Based on this, we now report for the first time the supramolecular self-assembly of 3D lightweight nanocellulose aerogels using carboxylated ginger cellulose nanofibers and polyaniline (PANI) in a green aqueous medium. A possible supramolecular self-assembly of the 3D conductive supramolecular aerogel (SA) was provided, which also possessed mechanical flexibility, shape recovery capabilities, and a porous networked microstructure to support the conductive PANI chains. The lightweight conductive SA with hierarchically porous 3D structures (porosity of 96.90%) exhibited a high conductivity of 0.372 mS/cm and a larger area-normalized capacitance (C_s) of 59.26 mF/cm^2, which is 20 times higher than other 3D chemically cross-linked nanocellulose aerogels, fast charge−discharge performance, and excellent capacitance retention. Combining the flexible SA solid electrolyte with low-cost nonwoven polypropylene and PVA/H_2SO_4 yielded a high normalized capacitance (C_m) of 291.01 F/g without the use of adhesive that was typically required for flexible energy storage devices. Furthermore, the supramolecular conductive aerogel could be used as a universal sensitive sensor for toxic gas, field sobriety tests, and health monitoring devices by utilizing the electrode material in lightweight supercapacitor and wearable flexible devices.

KEYWORDS: *supramolecular self-assembly, cellulose nanofiber aerogels, polyaniline, supercapacitors, sensors*

1. INTRODUCTION

Cellulose is the most abundant and renewable material on earth. Nanocellulose extracted from various cellulose materials possesses high mechanical strength, surface hydroxyl groups for chemical modification, low density, and biocompatibility.[1,2] It can be further combined with functional nanoparticles or conductive polymers for sustainable energy storage and sensor devices.[3] The flexible three-dimensional (3D) nanocellulose aerogels with a highly porous network structure are promising systems for use in supercapacitors, energy storage devices, sensors, lithium−sulfur batteries, and flexible personal care devices.[4−6] However, pure nanocellulose aerogels with more hydrophilic groups will lead to the poor structural stability in a green aqueous medium and further restrict their combination with electrode materials for the above related applications.[6,7] To solve the above problems, Yang et al.[7] used chemical modification techniques to prepare two types of cellulose nanocrystals (CNCs) containing aldehyde and hydrazide groups, which were then chemically cross-linked to form 3D lightweight CNC aerogels with a stable structure. These shape-

Received: April 14, 2019
Accepted: June 20, 2019
Published: June 20, 2019

DOI: 10.1021/acsami.9b06527
ACS Appl. Mater. Interfaces 2019, 11, 24435−24446

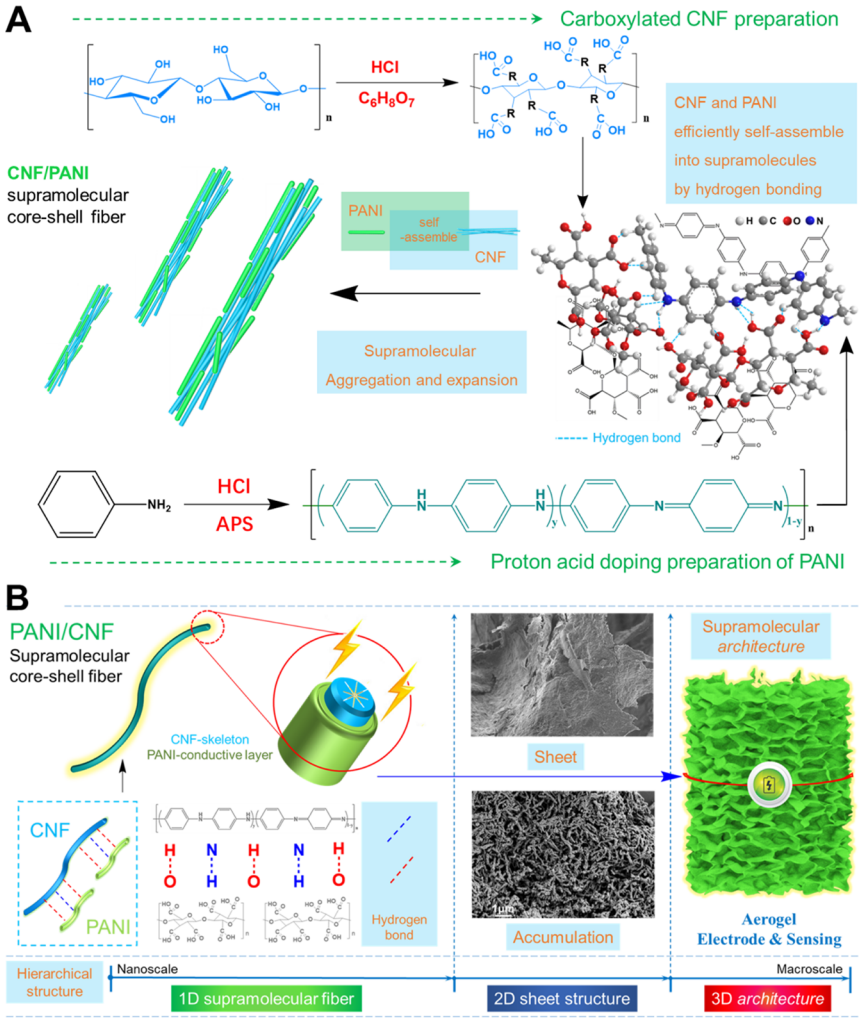

Figure 1. (A) Schematic synthesis of 2D supramolecular fibers and (B) supramolecular assembly process and their 2D structural arrangement to form 3D aerogels.

recoverable substrates were blended with polypyrrole (PPy), PPy-carbon nanotubes (PPy-CNT), and manganese dioxide (MnO_2) and used as electrode materials for supercapacitors. 3D CNC hybrid aerogels displayed excellent capacitance retention at high charge−discharge rates due to the abundance of a multiple channel structure for electronic and ionic diffusion of charges. However, these hybrid aerogels displayed unfavorable area-normalized specific capacitance values of 2.14−3.32 mF/cm^2, which were caused by poor dispersion of capacitive materials on the low-aspect-ratio CNC with a reduced active electrochemical surface area.[7,8] Indeed, aldehyde- and hydrazide-based modifications with toxic monomers consume more hydroxy groups on the CNC, thus reducing the hydrogen bonds between the CNC and capacitive materials. The assembly of conductive polymers on nanocellulose with a high aspect ratio to form 3D lightweight nanocellulose aerogels in a green aqueous medium with a porous network structure, high specific capacitance, and sensor sensitivity is still a challenge.

Nature employs supramolecular self-assembly to organize many molecularly complex structures,[9,10] such as human tissues, molecular membranes, and gels.[11,12] Based on this, we now report for the facile and rapid hydrogen bond-induced supramolecular rapid self-assembly of 3D lightweight cellulose aerogels using carboxylated ginger cellulose nanofibers (CNFs) and polyaniline (PANI, as a model conductive polymer). The delocalized π-electrons along the backbone of conjugated conductive polymers (PANI) induce phase separation/aggregation and mechanical brittleness of a noncontinuous conductive polymer network within the gel matrix. In this study, high-aspect-ratio CNF and PANI combine to initiate supramolecular self-cross-linking into flexible aerogels with good structural stability and exhibit excellent synergy, imparting flexibility and toughness to the brittle PANI, as well as independent electrochemical and sensing performance.[13−15] In this strategy, the H atom of O−H on CNF forms hydrogen bonds with the N atom on PANI, and the H atom of N−H on PANI also forms hydrogen bonds with the O atom on CNF. The chemical structure of PANI and CNF ensured more enough hydrogen bonds, so they can quickly self-assemble into supramolecules (Figure 1, similar to DNA base pair structures[15]). PANI covers the overall structure of the SAs, and there is no problem of shedding. An added advantage of the one-step supramolecular assembly method is that binders, surface functionalization or chemical cross-linking, and carbon/metal supports[5,16] are not needed, which reduces the weight and improves the performance of the device.

The 3D conductive SA possesses mechanical flexibility, shape recovery capabilities, and a porous networked microstructure to support the conductive PANI chains, thus

DOI: 10.1021/acsami.9b06527
ACS Appl. Mater. Interfaces 2019, 11, 24435−24446

addressing the poor electrolyte diffusion encountered by the deposition and slurry impregnation methods for 2D carbon-based or conductive polymer supercapacitor devices.[17] In our previous study,[18] high-aspect-ratio carboxylated CNF extracted from biomass can be easily physically cross-linked into a bulk aerogel of the desired shape. They have a high porosity, large specific surface area, adjustable density, and rich hydrogen bond content. These properties lay the foundation for the above properties of 3D conductive SA. Therefore, the lightweight conductive SA possesses hierarchically porous 3D structures (porosity of 96.90%), high PANI content (increase of 66.67%), a larger area-normalized capacitance (C_s) of 59.26 mF/cm^2 (20 times higher than other 3D nanocellulose aerogels[7]), fast charge−discharge performance, and excellent capacitance retention. Combining the flexible SA solid electrolyte with low-cost nonwoven polypropylene (PP) and PVA/H_2SO_4 yielded a high normalized capacitance (C_m) of 291.01 F/g without the use of adhesive that is typically required for flexible energy storage devices. Furthermore, the highly sensitive SA gas sensors can detect low concentrations of chloroform, ethanol, formaldehyde, and toluene down to 10 ppm (typical test requirements for alcohol content for drivers in China). In addition, real-time monitoring of human vital signals, such as body movements and pulse, can be achieved. This flexible, nontoxic, and recyclable SA can be combined with textiles in smart wearable devices.

2. EXPERIMENTAL SECTION

2.1. Materials. Ginger fiber is isolated from natural ginger (length, 3−15 cm; diameter, 500−1000 μm); aniline (99%), citric acid ($C_6H_8O_7$, 99.8%), hydrochloric acid (HCl, 99.5%), ammonium persulfate (APS, 99.9%), sulfuric acid (H_2SO_4, 98%), and poly(vinyl alcohol) (PVA, M_w = 67,000) were purchased from Aladdin Industrial Corporation (Shanghai, China). Polypropylene (PP) nonwoven fabric was purchased from Zhigao Textile Factory (Yiwu, China).

2.2. Preparation of Carboxylated CNF. The preparation of CNF used the methods reported in our previous report.[1] Briefly, using the mixed acid method, $C_6H_8O_7$/HCl (3 M/6 M, 7:3, v/v) was added to Fischer esterified ginger fiber to obtain high-aspect-ratio carboxylated CNF; the CNF has a length of 3690 ± 550 nm, diameter of 25.6 ± 10.2 nm, carboxyl content of 1.18 ± 0.10 mmol/g, and zeta potential of −30.0 ± 3.0 mV.

2.3. Synthesis of Supramolecular CNF/PANI Fibers. First, 0.5 g of aniline was added to 50 mL of 1 M HCl, and then 0.5 g of APS was dissolved in 50 mL of 1 M HCl and slowly added to the aniline solution. Thereafter, the reaction was carried out at 0 ° C for 4 h in a freezing shaker, and finally, acetone was added to stop the reaction. PANI suspension was obtained by suction filtration. The CNF suspension was mixed with the PANI suspension for supramolecular assembly. The mass ratio of CNF/PANI is 1:1, 2:1, and 1:2, and the samples are named SupCP1/1, SupCP2/1, and SupCP1/2 according to the ratio of CNF/PANI, respectively.

2.4. Fabrication of Supramolecular CNF/PANI Aerogels for Flexible Electrode and Universal Sensor. The CNF/PANI nanocomposite fiber suspension (10%) was poured into a Teflon plate, frozen in liquid nitrogen, and placed in a freezer at −30 °C overnight. After being taken out, it was quickly placed in a freeze dryer and freeze-dried to obtain an SA. These porous aerogels can be used directly as sensors and electrodes for supercapacitors after compression under 1 MPa pressure using a press.

2.5. Fabrication of All-Solid Flexible Supercapacitors. Firstly, 6 g of H_2SO_4 was mixed with 60 mL of deionized water, followed by 6 g of PVA powder. The mixture was heated to 85 °C with stirring until the solution was clear. Second, the PP nonwoven fabric intermediate portion was immersed in the above hot mixed solution and taken out after 10 min. Immediately, after removal of the flexible electrolyte from mixed solution, two flexible SA electrodes were attached to both sides. Finally, the flexible supercapacitor was obtained under 0.1 MPa pressure using a press for 10 min and then ventilated at room temperature for 4 h to evaporate excess water. Two flexible all-solid supercapacitors were connected together using foamed nickel, charged at 3.0 V, and then connected to a 3.0 V blue LED using copper wires. The electrochemical performance of flexible all-solid supercapacitors was tested under normal and bent conditions.

2.6. Fabrication of Flexible Supramolecular Aerogel Gas Sensor and Supramolecular Aerogel Vital Sign Sensor. The supramolecular aerogel gas sensor (SAGS) directly used SA as a gas-sensitive material and connects two double-sided conductive copper tapes on the upper and lower sides for transmitting electrical signals. The supramolecular aerogel vital sign sensor (SAVS)/SA was attached to the PVA/PP nonwoven fabric and then compressed at 0.1 MPa to connect double-sided conductive copper tape at both ends of the SA.

2.7. Characterizations. *2.7.1. FE-SEM and TEM Characterization.* The morphology of supramolecular CNF/PANI fibers was observed by FE-SEM (JSM-5610, JEOL, Japan) at an accelerated voltage of 1.0 kV at room temperature. About 0.01 wt % cellulose nanofiber/polyaniline supramolecular fibers were dispersed in water, and the suspension was sonicated in an ice bath (S7500, Branson, USA) for 15 min, then deposited on a silicon wafer, and dried in an oven at 60 °C. Further, a well-dispersed CNF/PANI composite conductive fiber was observed by TEM (JEM-2100, JEOL, Japan). Approximately 0.001 wt % sediment of the aqueous suspension of CNF/PANI conductive fiber was deposited onto a copper grid.

2.7.2. UV Spectroscopy. The optical properties of the supramolecular CNF/PANI fibers were characterized in the wavelength interval between 200 and 800 nm by using an ultraviolet spectrophotometer (U-3900, HITACHI, Japan).

2.7.3. FTIR Spectroscopy. FTIR spectroscopy was recorded on a Nicolet IS50 (Thermo Fisher Scientific, USA). All samples were mixed with KBr particles into a sheet-like shape; the spectrometer was used for the absorption mode, and the wavelength range was 4000 to 400 cm^{-1}. For each spectrum, 2 cm^{-1} resolution and 32 spectra were taken. A separate background spectrum was collected and subtracted from the original spectrum of each sample.

2.7.4. Thermogravimetric Analysis (TGA). Thermal stability of CNF and supramolecular CNF/PANI fibers was studied using a thermogravimetric analyzer (TG209 F1, Netzsch, Germany). The samples (3−8 mg) were heated from 30 to 800 °C at a rate of 10 °C/min while using a dynamic nitrogen atmosphere to protect samples. The main thermal parameters, such as initial decomposition temperature (T_0) and maximum decomposition temperature (T_{max}), are recorded from the TGA curve.

2.7.5. Compression Performance Test. Supramolecular CNF/PANI aerogel compression performance was measured using a universal material testing machine (5943, Instron, U.K.).

2.7.6. Porosity. The porosities of the supramolecular CNF/PANI aerogel were calculated from the densities of the aerogel ($\rho_{aerogel}$), CNF (ρ_{CNF}), and PANI (ρ_{PANI})

$$\text{porosity}\ (\%) = \left\{1 - \left[\left(\rho_{\text{aerogel}} \times \frac{x}{6}\right)/\rho_{\text{CNF}}\right] - \left[\left(\rho_{\text{aerogel}} \times \frac{y}{6}\right)/\rho_{\text{PANI}}\right]\right\} \times 100\% \quad (1)$$

where $\frac{x}{6}$ is the weight ratio of CNF in an aerogel, and $\frac{y}{6}$ is the weight ratio of PANI in an aerogel. Among them, $x + y = 6$.

2.7.7. Electrochemical Measurements. CV and EIS studies were performed using a CHI660E electrochemical analyzer (CH Instruments, Inc., USA). The CV scan data was obtained in a 1.0 V voltage window using Na_2SO_4 as the electrolyte at a scan rate of 10−600 mV/s and H_2SO_4 as the electrolyte at a scan rate of 5−200 mV/s. The total capacitance $C = Q/\Delta V$ was calculated using half of the integrated area of the CV curve to obtain the charge Q, and then the charge Q was divided by ΔV. The mass-normalized capacitance and area-normalized capacitance of the supramolecular fibers were calculated by equations $C_m = C/2m$ and $C_s = C/S$, where m is the mass of the

DOI: 10.1021/acsami.9b06527
ACS Appl. Mater. Interfaces 2019, 11, 24435−24446

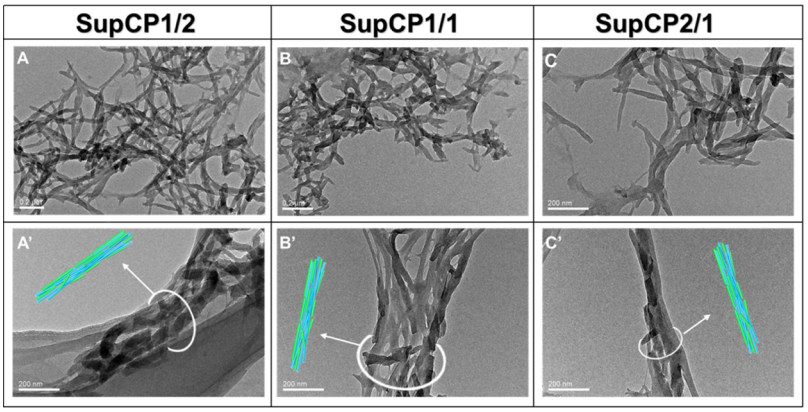

Figure 2. TEM images of (A, A′) SupCP1/1, (B, B′) SupCP1/2, and (C, C′) SupCP2/1. Scale bars: 200 nm.

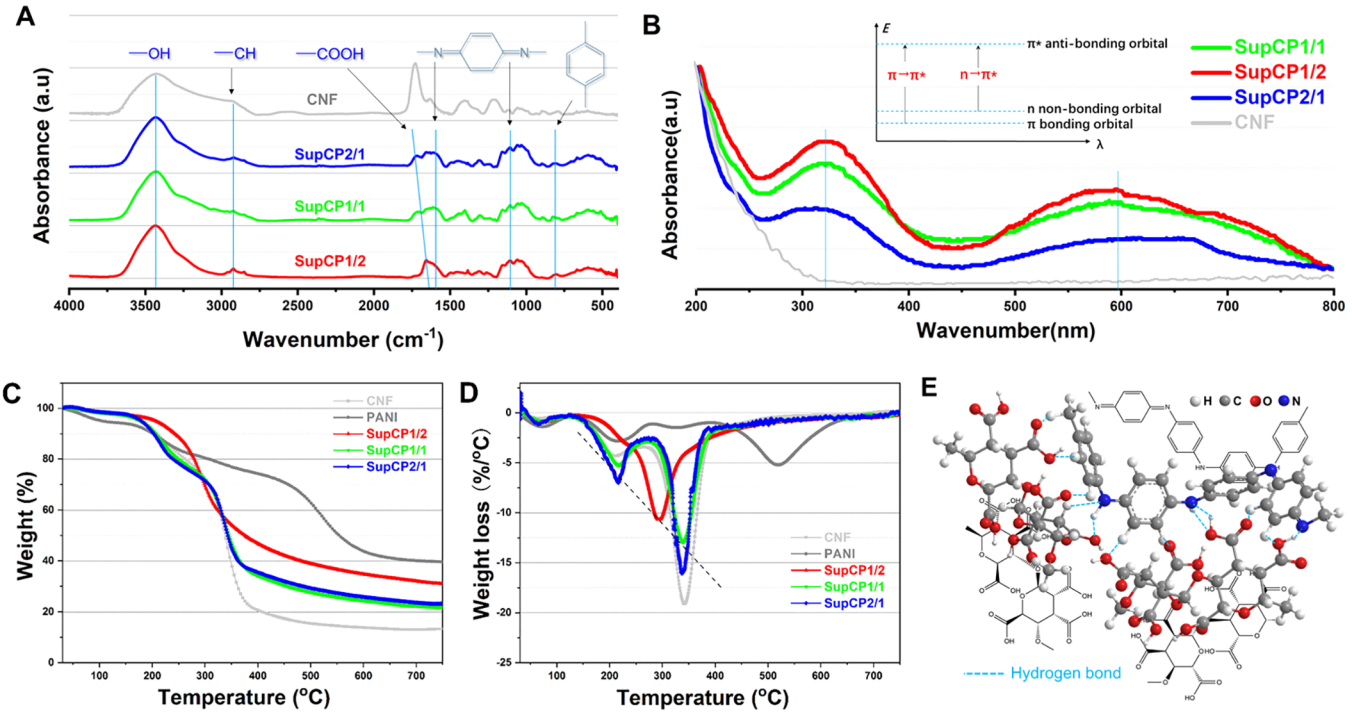

Figure 3. (A) FTIR spectra and characteristic peak labeling. (B) UV−vis spectra, $n \rightarrow \pi^*$ energy level transition, and $\pi \rightarrow \pi^*$ energy level transition diagram. (C, D) TG/DTG curves of pure CNF, PANI, and SupCP aerogels; the black dashed line in the figure indicates the best synergy between PANI and CNF in SupCP1/2. (E) Schematic diagram of the simulated supramolecular spatial 3D structure of CNF and PANI bonded to supramolecular fibers by hydrogen bonds.

electrode, and S is the geometric area of the electrode. The EIS measurement was performed in the frequency range of 0.1 Hz to 100 kHz. The constant current charge−discharge behavior and cycle stability of the supercapacitor battery were investigated between 0.5 and 4 A/g.

2.7.8. Gas Sensing, Finger Bending, and Pulse Sensing Tests. The SA was exposed to various sample gases (chloroform ($CHCl_3$), ethanol (C_2H_6O), etc.) to evaluate gas sensing performance. The difference in electrical resistance (ΔR; $\Delta R = R_{gas} - R_{base}$) between the supramolecular aerogel contact and off-gas atmosphere was recorded using an electrometer (34460A, Agilent, USA). SAVS was used to attach to the index finger joint to record the voltage change (ΔV; $\Delta V = V_{sense} - V_{base}$) of the finger bending. The SAVS was attached to the skin of the wrist artery to record the ΔV caused by the pulse.

3. RESULTS AND DISCUSSION

The structural formation of SAs had undergone three stages: (i) 1D supramolecular CNF/PANI (SupCP) fibers assembled via hydrogen bonds[19,20] that are formed into shell-like structures (Figure 1A) for electron transport. (ii) Supramolecular fibers were prepared from the stacking of 2D sheet structures, like slabs in a construction process. As the "core" of the composite fiber, the CNF functions as a support to align the PANI chains to yield a supramolecular structure for the conduction of electrons. After nanoscale fibers were self-assembled, they were aligned and stacked into 2D layers, similar to the slabs in the construction process. (iii) The ice between the sheet structures sublimes in vacuum, and these supramolecular fibers assemble, entangle, and connect together to form a supramolecular 3D aerogel with superior electrical conductivity (Figure 1B).

The effect of different ratios of CNF and PANI on the microstructure of supramolecular fibers was observed by FE-SEM (Figure S1). Overall, the brightness of the sample

DOI: 10.1021/acsami.9b06527
ACS Appl. Mater. Interfaces 2019, 11, 24435−24446

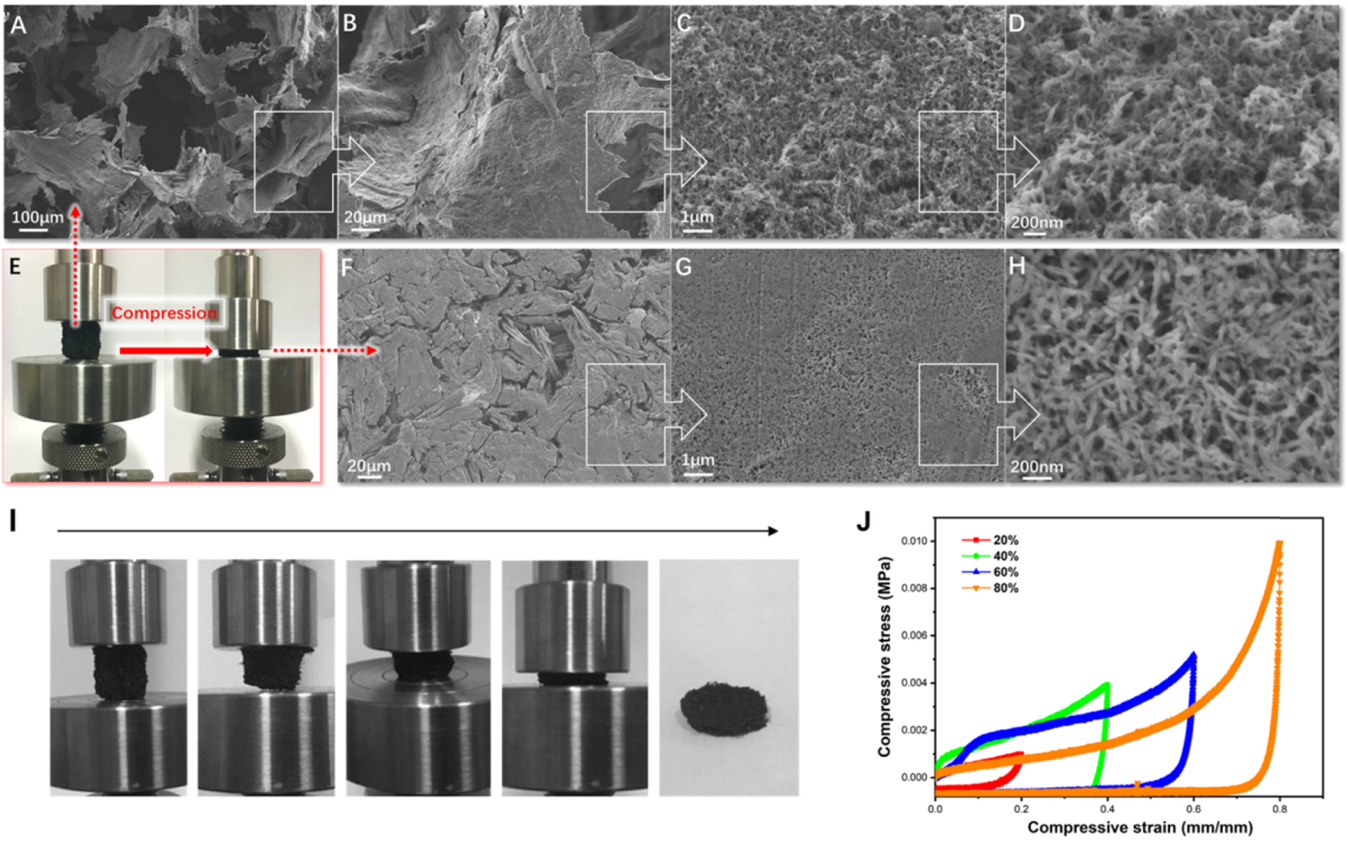

Figure 4. (A–D) FE-SEM images of SupCP1/2 pristine uncompressed aerogel (stepwise zoom microstructures). (E) Fabrication process and (F–H) FE-SEM images of compressed SupCP1/2 electrode (stepwise zoom microstructures). (I) Process of compressing SupCP1/2 aerogel into an electrode. (J) Mechanical recovery curve of aerogel at different compression ratios.

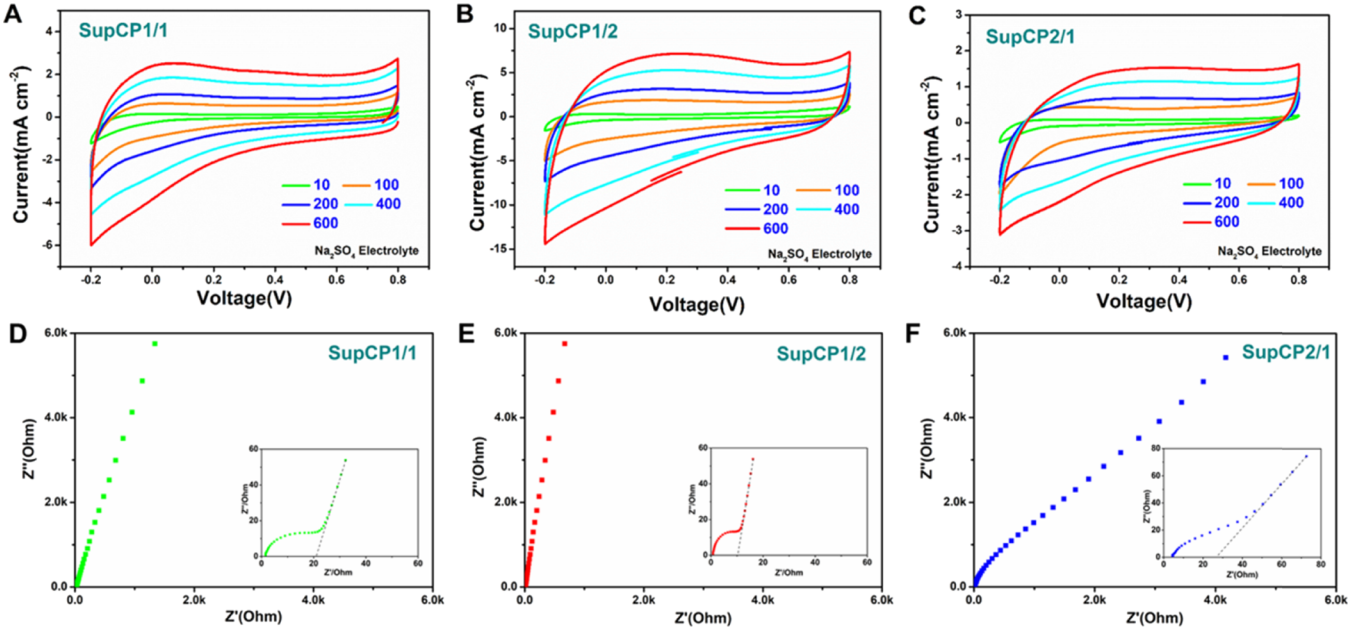

Figure 5. (A–C) CV data measured in 1 M Na_2SO_4 electrolyte at scan rates of 10–600 mV/s. (D–F) Nyquist plots of SupCP1/1 (D), SupCP1/2 (E), and SupCP2/1 (F). Inset: Magnified view of high-frequency region; the dotted line is the slope of the line in the low-frequency region, and the intersections with the Z' axis represent the internal resistance.

suggested uniform and well-dispersed CNF/PANI supramolecular fibers. The brighter areas represented the PANI chains, while the blurred regions corresponded to the nonconducting CNF. The resulting microstructure bonded with the electrolyte, enhancing the electron transport efficiency.[21] With increasing CNF content, the conductivity of the supramolecular fibers deteriorated, resulting in larger blurry regions. SupCP1/1 and SupCP1/2 seemed to possess

DOI: 10.1021/acsami.9b06527
ACS Appl. Mater. Interfaces 2019, 11, 24435–24446

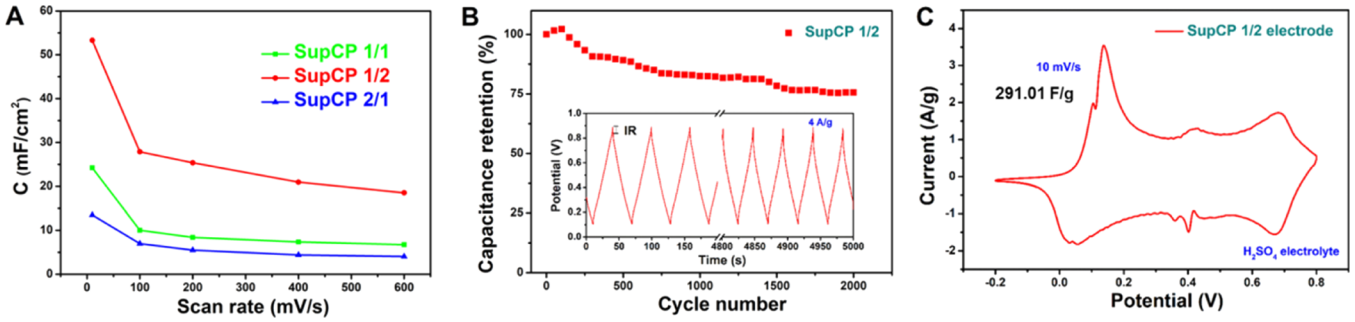

Figure 6. (A) Capacities at different scan rates. (B) Capacitance retention of SupCP1/2 after 2000 charge−discharge cycles (the inset is the charge−discharge curve). (C) CV curve of SupCP1/2 electrode in H_2SO_4 electrolyte.

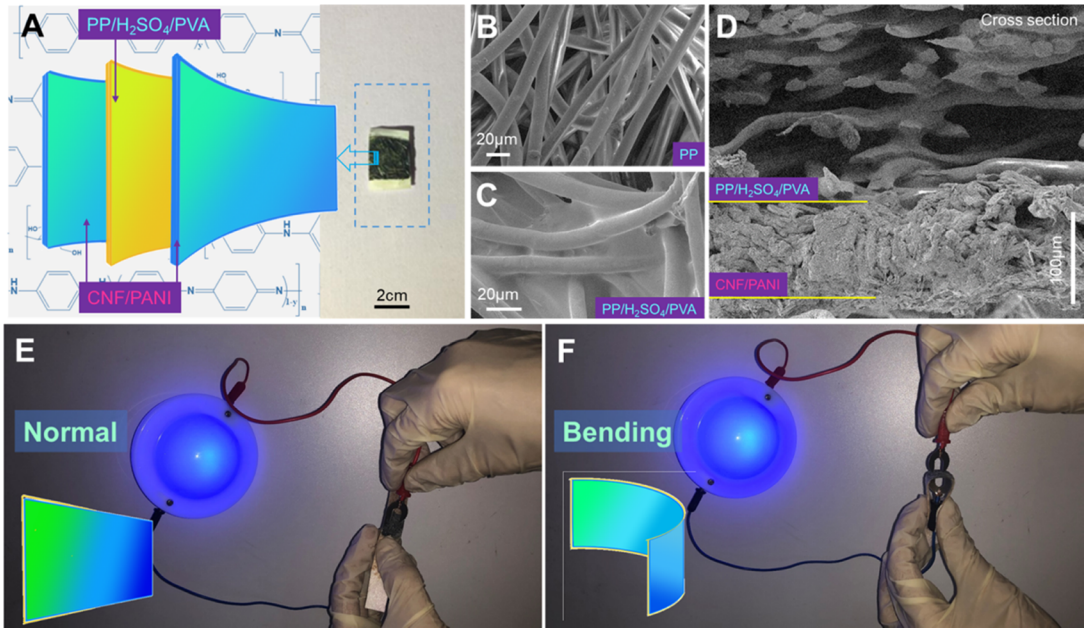

Figure 7. (A) Digital photo and structural diagram of flexible supercapacitor. (B, C) FE-SEM images of CNF/PANI aerogels and PP nonwoven fabric composite H_2SO_4/PVA solid electrolyte. (D) Cross section of the electrode and flexible solid electrolyte. (E, F) Digital photos of a flexible supercapacitor that illuminates a blue LED light in tiled and bent states; the outer casing enlarges the brightness of the LED light.

good conductivity (Figure S1A,A′,B,B′), while SupCP2/1 only had a few small areas with high brightness (Figure S1C,C′). High CNF contents would lead to uneven distribution of PANI, resulting in a lower coverage of the CNF by PANI. Compared with pure CNF and PANI (Figure S2), supramolecular fibers possessed 3D pore structures forming long-range continuous CNF structures resulting from the high aspect ratio of CNF. The self-assembly of supramolecular conductive fiber composites via hydrogen bonding not only improved the dispersion of PANI but also contributed to the formation of long-range structures by PANI. We noted that the supramolecular assembly processes were very efficient, as shown in Video S1 in the Supporting Information.

The microstructure of SupCP was further observed by TEM. The SupCP suspension was dispersed onto the ultrathin carbon film, and all samples had network or bundle structures, as shown by the difference in grayscale between CNF and PANI fibers. The diameter of the individual fibers was uniform at about 50 nm, confirming the FE-SEM results. As shown in the bundle structure, PANI and CNF tend to bind together in parallel. Compared with SupCP1/1 (Figure 2B,B′) and SupCP2/1 (Figure 2C,C′), SupCP1/2 (Figure 2A,A′) supramolecular fibers had a better morphology and higher PANI fiber ratio, which were beneficial to electronic transmission. TEM images of pure CNF and PANI are shown in Figure S3, which were similar as previous studies.[22,23]

In the FTIR spectra (Figure 3A), we observed the absorption peaks of the PANI aromatic ring at 1569 and 1120 cm^{-1} and the absorption peak of benzene aromatic carbon at 801 cm^{-1}.[24] The characteristic peaks of CNF (Figure 3A) at 3435, 2930, and 1735−1720 cm^{-1} corresponded to the stretching vibration of O−H, tensile vibration of C−H, and carboxyl groups (−COOH), respectively.[25] Interestingly, the carboxyl characteristic peak of CNF was red-shifted. With increasing PANI ratio, the carboxyl characteristic peaks of CNF shifted from 1735 cm^{-1} (SupCP2/1) to 1720 cm^{-1} (SupCP1/2) caused by an increase in the number of hydrogen bonds, and the increase in the electron cloud density reduced the frequency of C═O stretching vibration. When the PANI content was twice that of CNF, the C═O bond frequency reduced to 1720 cm^{-1} for SupCP1/2 since more PANI formed hydrogen bonds with the CNF carboxyl group. In general, intramolecular hydrogen bonds are not affected by concentration of various components, while intermolecular hydrogen bonds are concentration-dependent.[26,27] The above results indicated that CNF and PANI were connected with the

DOI: 10.1021/acsami.9b06527
ACS Appl. Mater. Interfaces 2019, 11, 24435−24446

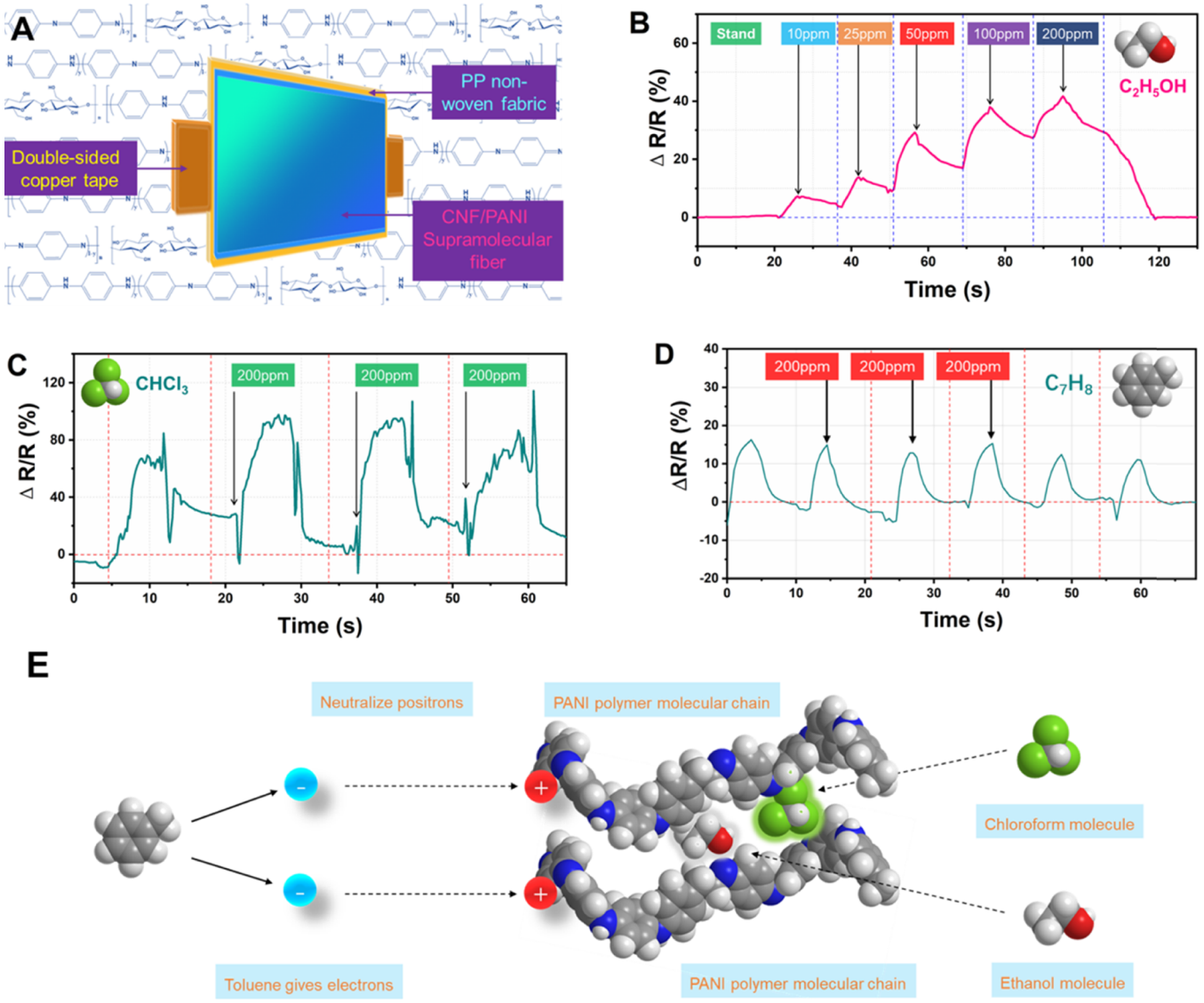

Figure 8. (A) Schematic diagram of a flexible SA gas sensor (SAGS) and flexible supramolecular aerogel vital sign sensor (SAVS), (B) resistance response signal of SAGS to 10−200 ppm C_2H_5OH gas, (C) resistance response signal of SAGS to $CHCl_3$ gas, and (D) resistance response signal of SAGS to C_7H_8 gas. (E) Schematic diagram of chloroform/ethanol-induced conformational changes in PANI and positrons of toluene electrons neutralizing PANI.

supramolecular fibers via intramolecular hydrogen bonds, and the corresponding functional groups and structures are identified in Figure 3A. Figure 3B shows that the three samples possessed similar UV absorption peaks, and the peak intensity increased with increasing PANI content. Compared to pristine CNF (Figure 3B), all samples displayed the characteristic absorption peak of PANI at around 225 and 315 nm for the $\pi \rightarrow \pi^*$ transition in the benzenoid segment and at 600 nm for the $n \rightarrow \pi^*$ transition within the quinoid structure.[28,29] The TG/DTG curves in Figure 3C,D show that the T_0 and T_{max} of SupCP aerogels were 143−192 °C and 295−339 °C, respectively (Table S1). At a higher CNF content, the thermodynamic properties of SupCP1/1 and SupCP2/1 were more similar to the pure CNF.[18] When the PANI content was higher than the CNF, the two large thermal degradation peaks of SupCP1/2 merged into one peak due to the supramolecular assembly of PANI on the CNF to form integrated fibers. Since CNF comprised the skeleton of supramolecular fibers, it played a crucial role in enhancing the thermal stability of PANI. A simulation of the molecular 3D networked structures of supramolecular fibers is shown in Figure 3E, where there were enough hydrogen, nitrogen, and oxygen atoms on the outside of the molecule to form hydrogen bonds. This could be the reason that induced the self-assembly of CNF and PANI into supramolecular fibers (Video S1, and the simulation of the respective 3D space structures of CNF/PANI in Figure S4).

To elucidate the effect of the complexation, we performed studies on the composite suspension after it was thoroughly mixed for 30 min. In Figure S5A−C, after 2 h of standing, the SupCP samples displayed layering, with the upper layer identified as light green and the lower layer as dark green. After 24 h, the upper layer became transparent, the lower layer was still dark green, and the layer was thinner and resembled flower-like quicksand under gentle agitation. This phenomenon was not observed for pure PANI and CNF suspensions. We postulated that PANI and CNF formed a large number of hydrogen bonds along their molecular side chains, thus

DOI: 10.1021/acsami.9b06527
ACS Appl. Mater. Interfaces 2019, 11, 24435−24446

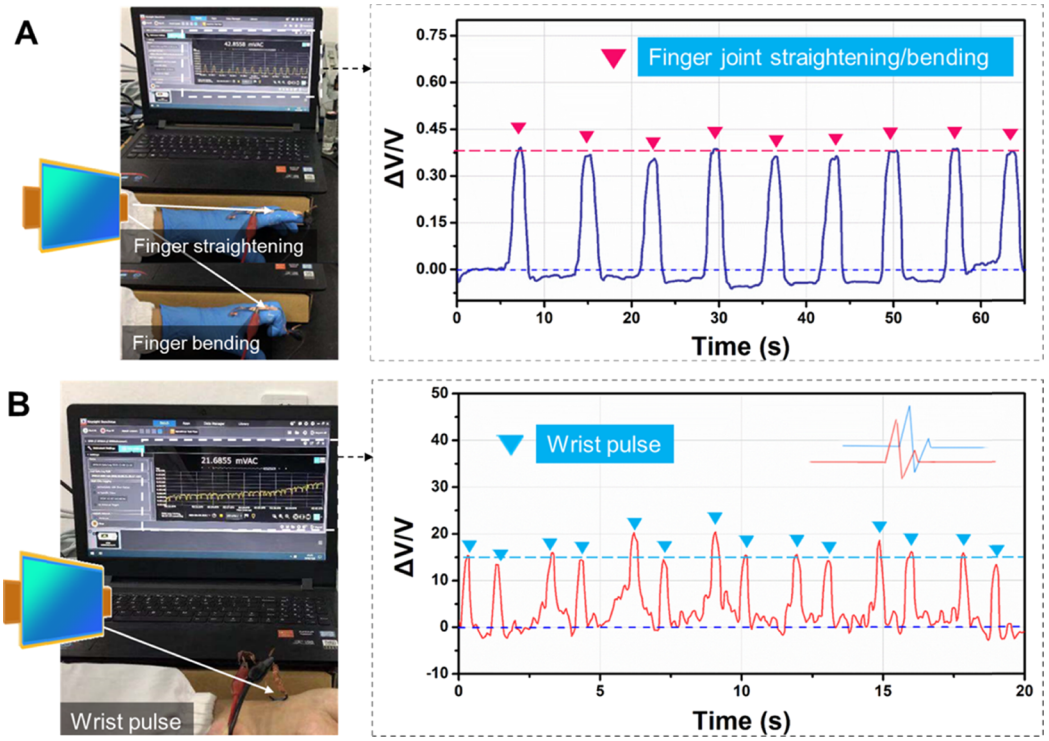

Figure 9. (A) Digital photos of flexible SAVS operation and voltage response signal of finger movement. (B) Digital photo of flexible SAVS-monitored wrist pulse and voltage response signal. Related tests shown in Videos S2 and S3 in the Supporting Information.

reducing the electrostatic repulsion. As a result, the supramolecular fibers sedimented to the bottom, while the weak electrostatic repulsion maintained the flower-like quicksand character. After freeze-drying (Figure S5D), PANI could not form an aerogel,[30] where dried powder adhered to the Teflon mold, while the other samples formed aerogels with hierarchical porous 3D structures. Figure S5E shows the zeta potential as a function of time after mixing, and the initial zeta potential of the CNF was negative. After mixing with the positively charged PANI, the zeta potential became positive. After a process of rapid integration into supramolecules, the zeta potential value reaches about zero. Thus, the CNF functioned as an aerogel skeleton to construct 3D supramolecular architectures for the supramolecular assembly of PANI dispersion. The CNF/PANI supramolecular aerogels possessed a smaller volume than a pure CNF aerogel due to the strong interaction between amino groups on PANI and the anionic functional groups on CNF that yielded a smaller and robust aerogel with excellent shape recovery even under 80% compression (Figure 4I,J). A higher ratio of PANI resulted in a smaller volume of aerogels, as shown in Figure S5D. In Table S1, the SupCP aerogel possessed a low density of 37.16−51.45 mg/cm^3 and high porosity of 94.65−96.90%. SupCP1/2 displayed the highest conductivity and relatively smaller density and porosity due to the large volume shrinkage. In summary, the high porosity and conductivity of 3D SupCP aerogels with excellent electrochemical performance and low density have advantages in lightweight supercapacitors and sensors.

Figure 4A−D shows the FE-SEM images at different magnifications of a SupCP1/2 pristine uncompressed aerogel: sheet-like structures inside the aerogel, supramolecular fibers organized on the sheet, and supramolecular fibers with nanoscale pores (20−150 nm) formed within the 3D structure. Most notably, the supramolecular conductive fibers were uniformly distributed and intertwined to form the pore structures. At a lower magnification (Figure 4C), the supramolecular conductive fibers were evenly distributed within the 3D aerogel structure, which was difficult to achieve previously.[7] There was no reported study on the preparation of well-distributed PANI dispersion in a 3D aerogel structure.[31−35] When compressed under moderate pressure (Figure 4E), the SA maintained good integrity without collapse (Figure 4I). Moreover, from the mechanical curve, the SA had a certain recovery performance (Figure 4J), which was beneficial to protect the composite structure of the supramolecular fiber from being destroyed. The SupCP electrode loosens its macroporous structure, maintaining its nanoscale pores, and the supramolecular conductive fibers were still regularly arranged like cute fluff (Figure 4F−H). These nanoscale pores facilitated the connection and ion conduction between the electrode and solid electrolyte (PP nonwoven fabric/H_2SO_4/PVA). The deformability of the aerogel function created structures that promoted the electrolyte contact and ion conduction necessary for their use as flexible sensors and capacitor electrodes.

The unique supramolecular structures of the SupCP aerogels, high electroactive material loading (66.67 wt % SupCP1/2 total electrode mass), and high porosity could synergistically enhance the supercapacitor performance. The CV curves in Figure 5A−C show that all three samples possessed a boxed or box-like CV shape, suggesting good capacitive behavior. The characteristic redox peak of PANI was evident on the CV curve, indicating the transition between the different redox states of PANI on the SupCP fiber surface.[36] Among them, SupCP1/2 displayed a CV curve closest to the box shape with the best symmetry, which was in agreement with SupCP1/2 possessing the best capacitive behavior. The

DOI: 10.1021/acsami.9b06527
ACS Appl. Mater. Interfaces 2019, 11, 24435−24446

current response profiles of SupCP1/1 and SupCP1/2 were linearly related to the scan rates, but the SupCP2/1 exhibited fluctuating current responses when the scan rate was increased from 100 to 200 mV/s. More importantly, both SupCP1/1 and SupCP1/2 could maintain the capacitive behavior at scan rates up to 600 mV/s, which was higher than the highest scan rates of other cellulose-based supercapacitors or polyaniline supercapacitors, most of which were significantly lower than 500 mV/s.[37−40] The excellent capacitance behavior at high scan rates was attributed to the rapid diffusion and good transport of electrolyte ions through the highly porous networks. The ion transport performance and internal impedance of the SupCP aerogels were examined by EIS and Nyquist plots (Figure 5D−F). In the low-frequency region, the Nyquist plots of SupCP1/1 and SupCP1/2 were nearly perpendicular to the Z' axis, confirming the ideal capacitive behavior caused by the finite diffusion length.[41] The excellent capacitive performance was due to the hierarchical porous aerogel structure of the supramolecular fibers, and the internal pores or paths of supramolecular aerogels could promote the transport of ions (Table S1 and Figure 4). In the high-frequency region, the intercepts of the Nyquist plot on the Z' axis corresponded to the equivalent series resistance (ESR) of the materials,[42] and the ESR values of SupCP aerogels were 10.2 to 26.9 Ω, with low electrical conductivity (Table S1), confirming the good contact with the electrolyte that provided the 3D pathways for electron transport.[43] Therefore, we assembled the SupCP aerogels into supercapacitor electrodes and ultrasensitive sensors to verify their excellent performance.

The area-normalized capacitance (C_s) was calculated from the CV curves. In Figure 6A, SupCP1/2 possessed the largest C_s, while smaller C_s values of SupCP1/1 and SupCP2/1 were observed. At a scan rate of 10 mV/s, the C_s values of SupCP1/2, SupCP1/1, and SupCP2/1 were 59.26, 24.24, and 13.49 mF/cm^2, respectively. The C_s value of SupCP1/2 was 3.32 mF/cm^2 higher than the chemically modified CNC aerogel electrode,[7] 45 mF/cm^2 larger than that of the CNF aerogel with Ag/PANI,[44] and 11.8 times greater than the carbon aerogel prepared after carbonization of bacterial cellulose (4.5 mF/cm^2).[45] Figure 6B shows that, after 2000 charge−discharge cycles, the capacitor retention rate of SupCP1/2 remained at 75.6% with good symmetry. The IR drop was only about 0.1 V, confirming that the SupCP1/2 electrode possessed good cycle stability, small equivalent series resistance, and fast charge−discharge performance. The excellent C_s values were due to negligible chemical interference (catalyst, chemical modifier) and uniform hierarchical pores inside the supramolecular aerogels. The addition of a catalyst or chemical modifier will contaminate the chemical environment/contact on the surface or inside the electrode, disrupting the electrolyte and electron transport, which reduced the electrochemical performance of the electrode.[46,47] The physically cross-linked carboxylated CNF aerogels described in this study did not display the above shortcomings since good PANI dispersion and self-assembly were achieved, yielding an improved electrochemical performance.

To manufacture a flexible supercapacitor, we chose a PP nonwoven composite PVA/H_2SO_4 solid electrolyte, and the performance of the SupCP electrode in the H_2SO_4 electrolyte was evaluated first. The CV curve in Figure 6C shows three pairs of redox peaks in the SupCP1/2 electrode. These nearly symmetrical redox peaks suggested a rapid electron transfer and enhanced reversible redox reaction.[48] An outstanding normalized capacitance (C_m) of 291.01 F/g was achieved, exceeding most cellulose-based or carbonized cellulose-based supercapacitor electrode materials.[49−52] The SupCP series showed that the increase in the redox current with scan rates (Figure S6) confirmed their excellent rate capability and cycle performance related to rapid ion motion and redox reaction.[53]

We designed a sandwich-type flexible supercapacitor by compressing a SupCP1/2 aerogel on both sides of the ultrathin PP/H_2SO_4/PVA flexible electrolyte (Figure 7A). This novel structure not only ensured the flexibility of the supercapacitor but also imparted a high degree of stability and mechanical strength. In Figure 7B,C, H_2SO_4/PVA was filled into the pores of the PP nonwoven fabric, and then the three components were integrated into one flexible electrolyte interlayer with a fiber diameter of 1 to 5 μm. This configuration facilitated the diffusion of ions and electrons. Figure 7D shows that the ultrathin flexible electrolyte was closely attached to the SupCP1/2 electrode, and this significantly reduced the electrical resistance between the interfaces and improved the electrochemical performance of the flexible supercapacitor.[54] To verify the performance of the flexible supercapacitor, we connected two flexible all-solid supercapacitors to a blue LED light (Figure 7E,F), where the flexible supercapacitors were capable of activating the LED in a normal or bent state. Moreover, the brightness of the LED did not change, demonstrating that the bending state did not affect the electrochemical performance of the flexible all-solid supercapacitor. This means that this flexible supercapacitor could be used as a stand-alone or portable micropower supply. More promisingly, this flexible supercapacitor could work without the use of adhesive, current collectors, or other auxiliary materials.

We designed the original SA for the use as a gas sensor and a moderately compressed supramolecular aerogel for flexible sensors (Figure 8A). The sensors in this study are mainly aimed at detecting living environment gases, and volatile organic compounds (VOCs), which are easily passively contacted in life such as chloroform, ethanol, toluene, and formaldehyde, are selected. Drinking water (China still uses sodium hypochlorite to disinfect tap water) and automobile exhaust contain chloroform, formaldehyde and toluene are present in decorative coatings and new furniture, and drunk drivers will exhale ethanol. The resistance response of the SAGS was responsive to C_2H_5OH, $CHCl_3$, C_7H_8 (Figure 8B−D), and CH_2O (Figure S7), but the response curves were different. In monitoring 200 ppm $CHCl_3$, the SAGS displayed very sharp response peaks, while the resistance response signal for 10−200 ppm C_2H_5OH was triangular in shape. With increasing C_2H_5OH concentration, the resistance of the SAGS increased, and the SAGS possessed a significant resistance response signal in response to 10 ppm C_2H_5OH, which was close to the metal nanowire/nanobelt sensor,[55] satisfying the test requirements of a commercial sensor using for field sobriety tests (FSTs).[56] SAGS also has a resistance response to toluene and formaldehyde gases but is not sensitive to changes in concentration. Chloroform and ethanol molecules attack the N−H site on PANI, causing the two polymer chains of PANI to swell. The conformational change and swelling of the polymer chains cause the transport of carriers to be hindered, resulting in an increase in electrical resistance. When the SAGS is taken out of the VOC gas, the conductive path begins to recover, and the resistance value returns to the initial state or near the initial state.[57−59] On the other hand, the toluene

DOI: 10.1021/acsami.9b06527
ACS Appl. Mater. Interfaces 2019, 11, 24435−24446

polymer chain entering PANI will generate electrons, neutralize positrons, and reduce the concentration of positive charge carriers in PANI, resulting in increased resistance.[60] This had different peak shape changes for different gases, but unfortunately, SAGS cannot distinguish which component of a multicomponent gas. Compared with fuel cell-type (electrochemical type) and semiconductor-type commercial ethanol sensors, the SAGS of this study has the advantages of convenient use and low cost, but the detection concentration lower limit is inferior to the commercial ethanol sensor. In general, SAGS can be made into a wearable sensor or embedded in the interior of a car, which has great potential for detecting drunk driving.

SAVS was prepared by pressing a supramolecular aerogel with PVA/PP nonwoven fabric, and the electrical signals were transmitted using a double-sided conductive copper tape (Figure 8A). The bending dynamic tests simulating the motion of the finger were performed by attaching the sensor to the finger joint (Figure 9A and Video S2). During the finger movement, the voltage yielded a distinct elevated voltage signal. In repeated tests, SAVS exhibited a regular and effective voltage response signal. Figure 9B and Video S3 show the heartbeat sensing test at the wrist of human body, and the digital multimeter recorded the real-time voltage signal of the human pulse, even though the pulse at the wrist was extremely weak. The SAVS developed in the study was capable of measuring pulse signals, indicating a very sensitive surface contact behavior.

4. CONCLUSIONS

In summary, this study was inspired by natural life to develop an unconventional method for the preparation of conductive cellulose-based aerogels in aqueous medium. The capacitive active material was no longer simply loaded in the cellulose aerogel but was linked into a supramolecular fiber with nanocellulose by bidirectional hydrogen bonding and constructed into an aerogel structure. We have observed that rapid supramolecular self-assembly of self-cross-linking conductive aerogels exhibited unprecedented uniformity at microscopic scales. In this case, PANI participated in the skeleton of the aerogel and provided a continuous fast path for electron conduction. Moreover, CNF/PANI SA had excellent synergistic and electrochemical properties, which exhibited great application potential in flexible supercapacitor electrodes. In the test of sensing performance, SA can not only monitor different gas concentration changes in the external environment but can also monitor human motion signals and pulse beat signals in different ways. This research provides a low-cost and rapid production solution for the development of wearable devices, especially flexible supercapacitors and sensors.

■ ASSOCIATED CONTENT

Supporting Information

The Supporting Information is available free of charge on the ACS Publications website at DOI: 10.1021/acsami.9b06527.

FE-SEM images of SupCP1/1, SupCP1/2, and SupCP2/1; FE-SEM images of cellulose nanofibers (CNFs) and polyaniline (PANI); TEM images of CNF and PANI; modification reaction of carboxylated CNF and its 3D space structure, PANI 3D space structure, and schematic diagram of the 3D space connecting CNF and PANI through hydrogen bonding; digital photos of the standing process of PANI, SupCP1/1, SupCP1/2, SupCP2/1, and CNF, digital photo of the aerogel formed after freeze drying, and zeta potential change versus time during the preparation of SupCP1/1, SupCP1/2, and SupCP2/1 by adding PANI into CNF; CV curves of SupCP1/2 tested for electrochemical performance by a three-electrode method in a sulfuric acid electrolyte at scan rates of 5, 50, and 200 mV/s; resistance response signal monitored by SAGS in formaldehyde gas and resistance response signal monitored by the SAVS at a pressure of 100 N; physical and thermodynamic parameters of SupCP1/1, SupCP1/2, and SupCP2/1 (PDF)

Polyaniline dripping into water and supramolecular rapid self-assembly process observed under the microscope (MP4)

Finger bending sensing (MP4)

Wrist pulse (heartbeat) sensing (MP4)

■ AUTHOR INFORMATION

Corresponding Authors

*E-mail: phdyu@zstu.edu.cn. Tel.: 86 571 86843618. Fax: 86 571 86843619 (H.-Y.Y.).

*E-mail: mkctam@uwaterloo.ca. Tel: 1-519-888-4567x38339. Fax: 1-519-888-4347 (K.C.T.).

ORCID

Duan-Chao Wang: 0000-0002-3133-4041

Hou-Yong Yu: 0000-0002-6543-5924

Kam (Michael) Chiu Tam: 0000-0002-7603-5635

Qingqing Ni: 0000-0001-9362-2148

Notes

The authors declare no competing financial interest.

■ ACKNOWLEDGMENTS

The work is supported by the Key Program for International S&T Innovation Cooperation Projects of China (2016YFE0131400), the Candidates of Young and Middle Aged Academic Leader of Zhejiang Province, and the Young Elite Scientists Sponsorship Program by CAST (2018QNRC001). The authors thank the University of Waterloo for the technical support, Yuhang Wu for TEM characterization, Xuemeng Fan for the 3D heart drawing, and Yuanbo Xie for the 3D aerogel drawing.

■ REFERENCES

(1) Moon, R. J.; Martini, A.; Nairn, J.; Simonsen, J.; Youngblood, J. Cellulose Nanomaterials Review: Structure, Properties and Nanocomposites. *Chem. Soc. Rev.* **2011**, *40*, 3941.

(2) De France, K. J.; Hoare, T.; Cranston, E. D. Review of Hydrogels and Aerogels Containing Nanocellulose. *Chem. Mater.* **2017**, *29*, 4609.

(3) Wang, Z.; Tammela, P.; Strømme, M.; Nyholm, L. Cellulose-Based Supercapacitors: Material and Performance Considerations. *Adv. Energy Mater.* **2017**, *7*, 1700130.

(4) Ding, Q.; Xu, X.; Yue, Y.; Mei, C.; Huang, C.; Jiang, S.; Wu, Q.; Han, J. Nanocellulose-Mediated Electroconductive Self-Healing Hydrogels with High Strength, Plasticity, Viscoelasticity, Stretchability, and Biocompatibility toward Multifunctional Applications. *ACS Appl. Mater. Interfaces* **2018**, *10*, 27987−28002.

(5) Xiong, R.; Hu, K.; Grant, A. M; Ma, R.; Xu, W.; Lu, C.; Zhang, X.; Tsukruk, V. V. Ultrarobust Transparent Cellulose Nanocrystal-Graphene Membranes with High Electrical Conductivity. *Adv. Mater.* **2016**, *28*, 1501−1509.

DOI: 10.1021/acsami.9b06527
ACS Appl. Mater. Interfaces 2019, 11, 24435−24446

(6) Quan, P.; Tang, J.; Huang, H.; Liang, X.; Connor, H.; Tam, K. C.; Nazar, L. F. A Nitrogen and Sulfur Dual-Doped Carbon Derived from Polyrhodanine@ Cellulose for Advanced Lithium−Sulfur Batteries. *Adv. Mater.* **2015**, *27*, 6021−6028.
(7) Yang, X.; Shi, K.; Zhitomirsky, I.; Cranston, E. D. Cellulose Nanocrystal Aerogels as Universal 3D Lightweight Substrates for Supercapacitor Materials. *Adv. Mater.* **2015**, *27*, 6104−6109.
(8) Toupin, M.; Brousse, T.; Bélanger, D. Influence of Microstucture on the Charge Storage Properties of Chemically Synthesized Manganese Dioxide. *Chem. Mater.* **2002**, *14*, 3946−3952.
(9) Wieghold, S.; Li, J.; Simon, P.; Krause, M.; Avlasevich, Y.; Li, C.; Garrido, J. A.; Heiz, U.; Samorì, P.; Müllen, K.; Esch, F.; Barth, J. V.; Palma, C.-A. Photoresponse of Supramolecular Self-Assembled Networks on Graphene−Diamond Interfaces. *Nat. Commun.* **2016**, *7*, 10700.
(10) Yan, D.; Zhou, Y.; Hou, J. Supramolecular Self-Assembly of Macroscopic Tubes. *Science* **2004**, *303*, 65−67.
(11) Mattia, E.; Otto, S. Supramolecular Systems Chemistry. *Nat. Nanotechnol.* **2015**, *10*, 111.
(12) Ke, Y.; Ong, L. L.; Shih, W. M.; Peng, Y. Three-Dimensional Structures Self-Assembled from DNA Bricks. *Science* **2012**, *338*, 1177−1183.
(13) Huang, J.; Virji, S.; Weiller, B. H.; Kaner, R. B. Polyaniline Nanofibers: Facile Synthesis and Chemical Sensors. *J. Am. Chem. Soc.* **2003**, *125*, 314−315.
(14) Ye, S.; Ma, C.; Peng, L.; Yu, G. Conductive "Smart" Hybrid Hydrogels with PNIPAM and Nanostructured Conductive Polymers. *Adv. Funct. Mater.* **2015**, *25*, 1219−1225.
(15) Vyborna, Y.; Vybornyi, M.; Rudnev, A. V.; Häner, R. DNA-Grafted Supramolecular Polymers: Helical Ribbon Structures Formed by Self-Assembly of Pyrene-DNA Chimeric Oligomers. *Angew. Chem., Int. Ed.* **2015**, *54*, 7934−7938.
(16) Zhang, Y.; Li, L.; Zhang, L.; Ge, S.; Yan, M.; Yu, J. In-Situ Synthesized Polypyrrole-Cellulose Conductive Networks for Potential-Tunable Foldable Power Paper. *Nano Energy* **2017**, *31*, 174−182.
(17) Wang, G.; Zhang, L.; Zhang, J. A Review of Electrode Materials for Electrochemical Supercapacitors. *Chem. Soc. Rev.* **2012**, *41*, 797−828.
(18) Wang, D.; Yu, H.; Fan, X.; Gu, J.; Ye, S.; Yao, J.; Ni, Q. High Aspect Ratio Carboxylated Cellulose Nanofibers Cross-linked to Robust Aerogels for Superabsorption−Flocculants: Paving Way from Nanoscale to Macroscale. *ACS Appl. Mater. Interfaces* **2018**, *10*, 20755−20766.
(19) Zhang, Q.; Xu, W.; Sun, J.; Pan, Z.; Zhao, J.; Wang, X.; Zhang, J.; Man, P.; Guo, J.; Zhou, Z. Constructing Ultrahigh-capacity Zinc−Nickel−Cobalt Oxide@Ni$(OH)_2$ Core−Shell Nanowire Arrays for High-Performance Coaxial Fiber-Shaped Asymmetric Supercapacitors. *Nano Lett.* **2017**, *17*, 7552−7560.
(20) Yang, P.; Xiao, X.; Li, Y.; Ding, Y.; Qiang, P.; Tan, X.; Mai, W.; Lin, Z.; Wu, W.; Li, T.; Jin, H.; Liu, P.; Zhou, J.; Wong, C. P.; Wang, Z. L. Hydrogenated ZnO Core−Shell Nanocables for Flexible Supercapacitors and Self-Powered Systems. *ACS Nano* **2013**, *7*, 2617−2626.
(21) Sun, H.; Xu, Z.; Gao, C. Multifunctional, Ultra-Flyweight, Synergistically Assembled Carbon Aerogels. *Adv. Mater.* **2013**, *25*, 2554−2560.
(22) Zhou, D.; Song, W. L.; Fan, L. Z. Hollow Core−Shell SnO_2/C Fibers as Highly Stable Anodes for Lithium-Ion Batteries. *ACS Appl. Mater. Interfaces* **2015**, *7*, 21472−21478.
(23) Xia, C.; Chen, W.; Wang, X.; Hedhili, M. N.; Wei, N.; Alshareef, H. N. Highly Stable Supercapacitors with Conducting Polymer Core−Shell Electrodes for Energy Storage Applications. *Adv. Energy Mater.* **2015**, *5*, 1401805.
(24) Liu, Y.; Ma, Y.; Guang, S.; Xu, H.; Su, X. Facile Fabrication of Three-Dimensional Highly Ordered Structural Polyaniline−Graphene Bulk Hybrid Materials for High Performance Supercapacitor Electrodes. *J. Mater. Chem. A* **2014**, *2*, 813−823.
(25) Yu, H.; Qin, Z.; Liang, B.; Liu, N.; Zhou, Z.; Chen, L. Facile Extraction of Thermally Stable Cellulose Nanocrystals with a High Yield of 93% through Hydrochloric Acid Hydrolysis under Hydrothermal Conditions. *J. Mater. Chem. A* **2013**, *1*, 3938−3944.
(26) Fecko, C. J.; Eaves, J. D.; Loparo, J. J.; Tokmakoff, A.; Geissler, P. L. Ultrafast Hydrogen-Bond Dynamics in the Infrared Spectroscopy of Water. *Science* **2003**, *301*, 1698−1702.
(27) Klein, R. A. Electron Density Topological Analysis of Hydrogen Bonding in Glucopyranose and Hydrated Glucopyranose. *J. Am. Chem. Soc.* **2002**, *124*, 13931−13937.
(28) Barman, T.; Hussain, A. A.; Sharma, B.; Pal, A. R. Plasmonic Hot Hole Generation by Interband Transition in Gold-Polyaniline. *Sci. Rep.* **2015**, *5*, 18276.
(29) Chen, H.; Yu, P.; Zhang, Z.; Teng, F.; Zheng, L.; Hu, K.; Fang, X. Ultrasensitive Self-Powered Solar-Blind Deep-Ultraviolet Photodetector Based on All-Solid-State Polyaniline/MgZnO Bilayer. *Small* **2016**, *12*, 5809−5816.
(30) Baker, C. O.; Huang, X.; Nelson, W.; Kaner, R. B. Polyaniline Nanofibers: Broadening Applications for Conducting Polymers. *Chem. Soc. Rev.* **2017**, *46*, 1510−1525.
(31) Hashemi, M.; Rahmanifar, M. S.; El-Kady, M. F.; Noori, A.; Mousavi, M. F.; Kaner, R. B. The Use of an Electrocatalytic Redox Electrolyte for Pushing the Energy Density Boundary of a Flexible Polyaniline Electrode to A New Limit. *Nano Energy* **2018**, *44*, 489−498.
(32) Gong, K.; Hu, Q.; Xiao, Y.; Xiang, C.; Hu, L.; Ning, W.; Qiu, B.; Guo, Z. Triple Layered Core−Shell ZVI@ Carbon@ Polyaniline Composite Enhanced Electron Utilization in Cr (VI) Reduction. *J. Mater. Chem. A* **2018**, *6*, 11119−11128.
(33) Shi, H. Y.; Ye, Y. J.; Liu, K.; Song, Y.; Sun, X. A Long-Cycle-Life Self-Doped Polyaniline Cathode for Rechargeable Aqueous Zinc Batteries. *Angew. Chem., Int. Ed. Engl.* **2018**, *57*, 16359−16363.
(34) Aggas, J. R.; Harrell, W.; Lutkenhaus, J.; Guiseppi-Elie, A. Metal−Polymer Interface Influences Apparent Electrical Properties of Nano-Structured Polyaniline Films. *Nanoscale* **2018**, *10*, 672−682.
(35) Khan, N. A.; Yoo, D. K.; Jhung, S. H. Polyaniline-Encapsulated Metal−Organic Framework MIL-101: Adsorbent with Record-High Adsorption Capacity for the Removal of Both Basic Quinoline and Neutral Indole from Liquid Fuel. *ACS Appl. Mater. Interfaces* **2018**, *10*, 35639−35646.
(36) Wu, Q.; Xu, Y.; Yao, Z.; Liu, A.; Shi, G. Supercapacitors Based on Flexible Graphene/Polyaniline Nanofiber Composite Films. *ACS Nano* **2010**, *4*, 1963−1970.
(37) Zhou, K.; He, Y.; Xu, Q.; Zhang, Q. E.; Zhou, A. A.; Lu, Z.; Yang, L. K.; Jiang, Y.; Ge, D.; Liu, X. Y.; Bai, H. A Hydrogel of Ultrathin Pure Polyaniline Nanofibers: Oxidant-Templating Preparation and Supercapacitor Application. *ACS Nano* **2018**, *12*, 5888−5894.
(38) Li, W.; Gao, F.; Wang, X.; Zhang, N.; Ma, M. Strong and Robust Polyaniline-Based Supramolecular Hydrogels for Flexible Supercapacitors. *Angew. Chem., Int. Ed.* **2016**, *55*, 9196−9201.
(39) Wu, H.; Zhang, Y.; Yuan, W.; Zhao, Y.; Luo, S.; Yuan, X.; Zheng, L.; Cheng, L. Highly Flexible, Foldable and Stretchable Ni−Co Layered Double Hydroxide/Polyaniline/Bacterial Cellulose Electrodes for High-Performance All-Solid-State Supercapacitors. *J. Mater. Chem. A* **2018**, *6*, 16617−16626.
(40) Luo, H.; Dong, J.; Yang, Z.; Li, G.; Guo, R.; Zuo, G.; Ye, M.; Wang, Z.; Yang, Z.; Wan, Y. Constructing 3D Bacterial Cellulose/Graphene/Polyaniline Nanocomposites by Novel Layer-By-Layer *In Situ* Culture toward Mechanically Robust and Highly Flexible Freestanding Electrodes for Supercapacitors. *Chem. Eng. J.* **2018**, *334*, 1148−1158.
(41) Li, D.; Gong, Y.; Pan, C. Facile Synthesis of Hybrid CNTs/$NiCo_2S_4$ Composite for High Performance Supercapacitors. *Sci. Rep.* **2016**, *6*, 29788.
(42) Xu, H.; Wu, C.; Wei, X.; Gao, S. Hierarchically Porous Carbon Materials with Controllable Proportion of Micropore Area by Dual-Activator Synthesis for High-Performance Supercapacitors. *J. Mater. Chem. A* **2018**, *6*, 15340−15347.
(43) Zhao, J.; Jiang, Y.; Fan, H.; Liu, M.; Zhuo, O.; Wang, X.; Wu, Q.; Yang, L.; Ma, Y.; Hu, Z. Porous 3D Few-Layer Graphene-Like

DOI: 10.1021/acsami.9b06527
ACS Appl. Mater. Interfaces 2019, 11, 24435−24446

Carbon for Ultrahigh-Power Supercapacitors with Well-Defined Structure−Performance Relationship. *Adv. Mater.* **2017**, *29*, 1604569.
(44) Zhang, X.; Lin, Z.; Chen, B.; Zhang, W.; Sharma, A.; Gu, W.; Deng, Y. Solid-State Flexible Polyaniline/Silver Cellulose Nanofibrils Aerogel Supercapacitors. *J. Power Sources* **2014**, *246*, 283−289.
(45) Islam, N.; Li, S.; Ren, G.; Zu, Y.; Warzywoda, J.; Wang, S.; Fan, Z. High-Frequency Electrochemical Capacitors Based on Plasma Pyrolyzed Bacterial Cellulose Aerogel for Current Ripple Filtering and Pulse Energy Storage. *Nano Energy* **2017**, *40*, 107−114.
(46) Etacheri, V.; Haik, O.; Goffer, Y.; Roberts, G. A.; Stefan, I. C.; Fasching, R.; Aurbach, D. Effect of Fluoroethylene Carbonate (FEC) on The Performance and Surface Chemistry of Si-Nanowire Li-Ion Battery Anodes. *Langmuir* **2011**, *28*, 965−976.
(47) Ma, F. X.; Yu, L.; Xu, C. Y.; Lou, X. W. D. Self-Supported Formation of Hierarchical $NiCo_2O_4$ tetragonal Microtubes with Enhanced Electrochemical Properties. *Energy Environ. Sci.* **2016**, *9*, 862−866.
(48) Tang, L.; Ying, W.; Li, Y.; Feng, H.; Lu, J.; Li, J. Preparation, Structure, and Electrochemical Properties of Reduced Graphene Sheet Films. *Adv. Funct. Mater.* **2009**, *19*, 2782−2789.
(49) Hao, P.; Zhao, Z.; Tian, J.; Li, H.; Sang, Y.; Yu, G.; Cai, H.; Liu, H.; Wong, C. P.; Umar, A. Hierarchical Porous Carbon Aerogel Derived from Bagasse for High Performance Supercapacitor Electrode. *Nanoscale* **2014**, *6*, 12120−12129.
(50) Li, S.-C.; Hu, B.-C.; Ding, Y.-W.; Liang, H.-W.; Li, C.; Yu, Z.-Y.; Wu, Z.-Y.; Chen, W. S.; Yu, S.-H. Wood-Derived Ultrathin Carbon Nanofiber Aerogels. *Angew. Chem.* **2018**, *130*, 7203−7208.
(51) Xu, X.; Zhou, J.; Nagaraju, D. H.; Jiang, L.; Marinov, V. R.; Lubineau, G.; Alshareef, H. N.; Oh, M. Flexible, Highly Graphitized Carbon Aerogels Based On Bacterial Cellulose/Lignin: Catalyst-Free Synthesis and Its Application in Energy Storage Devices. *Adv. Funct. Mater.* **2015**, *25*, 3193−3202.
(52) Yu, M.; Li, J.; Wang, L. KOH-Activated Carbon Aerogels Derived from Sodium Carboxymethyl Cellulose for High-Performance Supercapacitors and Dye Adsorption. *Chem. Eng. J.* **2017**, *310*, 300−306.
(53) Xiong, T.; Lee, W. S. V.; Chen, L.; Tan, T. L.; Huang, X.; Xue, J. Indole-Based Conjugated Macromolecules as a Redox-Mediated Electrolyte for An Ultrahigh Power Supercapacitor. *Energy Environ. Sci.* **2017**, *10*, 2441−2449.
(54) Zhou, D.; He, Y.-B.; Liu, R.; Liu, M.; Du, H.; Li, B.; Cai, Q.; Yang, Q.-H.; Kang, F. In Situ Synthesis of a Hierarchical All-Solid-State Electrolyte Based on Nitrile Materials for High-Performance Lithium-Ion Batteries. *Adv. Energy Mater.* **2015**, *5*, 1500353.
(55) Liu, J.; Wang, X.; Peng, Q.; Li, Y. Vanadium Pentoxide Nanobelts: Highly Selective and Stable Ethanol Sensor Materials. *Adv. Mater.* **2005**, *17*, 764−767.
(56) Liu, G.; Chen, S.; Zeng, Z.; Cui, H.; Fang, Y.; Gu, D.; Yin, Z.; Wang, Z. Risk Factors for Extremely Serious Road Accidents: Results from National Road Accident Statistical Annual Report of China. *PLoS One* **2018**, *13*, No. e0201587.
(57) Zhang, X.; Qin, Z.; Liu, X.; Liang, B.; Liu, N.; Zhou, Z.; Zhu, M. Flexible Sensing Fibers Based on Polyaniline-Coated Polyurethane for Chloroform Vapor Detection. *J. Mater. Chem. A* **2013**, *1*, 10327−10333.
(58) Chiam, Y. S.; Lim, K. S.; Harun, S. W.; Gan, S. N.; Phang, S. W. Conducting Polymer Coated Optical Microfiber Sensor for Alcohol Detection. *Sensors Actuat. A: Phys.* **2014**, *205*, 58−62.
(59) Virji, S.; Huang, J.; Kaner, R. B.; Weiller, B. H. Polyaniline Nanofiber Gas Sensors: Examination of Response Mechanisms. *Nano Lett.* **2004**, *4*, 491−496.
(60) Li, W.; Hoa, N. D.; Cho, Y.; Kim, D.; Kim, J. S. Nanofibers of Conducting Polyaniline for Aromatic Organic Compound Sensor. *Sens. Actuators, B* **2009**, *143*, 132−138.

DOI: 10.1021/acsami.9b06527
ACS Appl. Mater. Interfaces 2019, 11, 24435−24446